Discover Applied Sciences

Research

Enhancing additive manufacturing for multi-layer samples: experimental analysis of aluminum sheet thickness and perforation geometry via fused filament fabrication

Amir H. Roohi[1] · Ali Sadooghi[2] · Amir Nourian[1] · Seyed Jalal Hashemi[2] · Babak Dashti[3] · Kaveh Rahmani[4]

Received: 20 August 2024 / Accepted: 5 March 2025
Published online: 19 March 2025

Abstract

The widespread integration of 3D printing technologies across diverse sectors, including prototyping and automotive industries, underscores their growing importance. This study aims to investigate the influence of aluminium sheet parameters (specifically, thickness, number, and perforation diameter) on the mechanical properties of multi-layer specimens fabricated using Fused filament fabrication (FFF) 3D printing. Polylactic acid sheets were deposited on both sides of aluminium sheets, creating a sandwich structure to enhance strength and flexibility. Aluminium sheets of varying thickness (1 mm and 2 mm) with perforations of 5 mm and 7 mm diameters were examined. Mechanical testing included flexural, compression, and impact assessments. Results from the flexural tests demonstrated that specimens reinforced with 2 mm thick aluminum sheets exhibited significantly higher force at failure. Compression testing revealed a notable increase in maximum compressive force for samples incorporating aluminium sheets. Charpy impact testing indicated an 882% improvement in impact strength for samples with a 2 mm aluminium sheet compared to those without. These findings highlight the critical role of aluminium sheet parameters in enhancing the mechanical performance of FFF-printed multi-layer structures. The study provides valuable insights for optimizing the design and fabrication of composite materials in additive manufacturing applications. The enhanced mechanical properties observed underscore the potential for these materials in sectors requiring robust and resilient components, such as aerospace and automotive industries.

Highlights

- Thicker aluminum sheet exhibits significantly higher force at failure in both bending and compression tests.
- More perforation size resulted in better adhesion between the PLA and aluminum sheets and more bending strength
- Samples with improved interlayer bonding demonstrated enhanced flexural strength and reduced delamination upon fractured

Keywords Additive manufacturing · 3D printing · Multi-layer sheets · Mechanical properties · Aluminium · PLA

✉ Ali Sadooghi, a.sadooghi@sru.ac.ir | [1]School of Science, Engineering, and Environment (SEE), University of Salford, Manchester M5 4WT, UK. [2]Department of Mechanical Engineering, National University of Skills (NUS), Tehran, Iran. [3] Department of Mechanical Engineering, Kar Higher Education Institute of Qazvin, Qazvin, Iran. [4]Executive Assistance, Basa Pars Sanat knowledge-based Company, Takestan, Iran.

1 Introduction

Multi-layer specimens signify an advancement in hybrid materials, integrating thin layers of polymer materials with metal sheets (primarily aluminium sheets). This innovative combination enables multi-layer samples to exploit the advantageous traits of both aluminium and polymer layers [1, 2]. Additive manufacturing, also known as 3D printing, is a novel fabrication method that produces tangible items from a geometric model by adding materials layer by layer [3, 4]. Traditional manufacturing methods, such as machining, frequently generate significant waste of raw materials due to chip formation. In contrast, the 3D printing method constructs the final piece by layering raw materials on top of one another, effectively eliminating residual manufacturing waste. In most cases, polymer and plastic filaments are the primary materials utilized in 3D printing. PLA is a degradable thermoplastic polymer widely utilized in biomedical and related fields due to its versatile properties; presenting in filament form with various color options, it is specifically designed for 3D printing [5, 6]. Production of samples using PLA is straightforward and compatible with various types of 3D printers.

Sometimes, in order to improve the mechanical and chemical properties of PLA, reinforced samples are produced, which are referred to as composite materials. In these materials, PLA is known as the base material, and the additives are called reinforcement materials. These reinforcement materials can be in powdered form at micro and nano sizes, and there are no restrictions on their composition. Other reinforcement materials have been used by researchers, including ceramics [7], wood, metals such as stainless steel [8], copper, bronze, and aluminum. Also, fibers such as glass and carbon fibers are also used to reinforce the base material [9]. This amalgamation augments its mechanical properties and expands its range of applications. Sandwich panels or multilayer sheets are structures made up of several different layers of metals and plastics, which have properties distinct from the constituent layers. Depending on the location and type of application of the sandwich panels, various metals can be used in their construction [10]. Aluminum being one of the most commonly used metal sheet in the structure of sandwich panels after steel. Aluminum sheets are characterized by their remarkable flexibility, outstanding resistance to corrosion, energy absorption capability, and a superior strength-to-weight ratio [11]. Moreover, aluminum sheets are recognized as among the most popular lightweight metal sheets, extensively utilized in the automotive and construction industries.

To date, numerous researchers have investigated the properties of PLA printed components as well as multi-layer sheets—e.g. Fiber Metal Laminates (FMLs): Zal et al. [12] experimentally investigated the mechanical properties of polyester/fibreglass/stainless FMLs. Their study focuses on FML sheets with a 2 mm thick intermediate layer of stainless steel 420 reinforced with six layers of woven and mat glass fibres. Various fibre angles (0°, 15°, 30°, and 45°) are examined. Results show that samples with fibres arranged at 0° exhibit the highest strength. Al Khawaja et al. [13] examine the mechanical properties of FFF-manufactured 3D printed components, focusing particularly on PLA samples. Their compression testing methodology assesses consistency across duplicate prints, revealing a high level of uniformity in the material's compressive behavior across multiple iterations. Rawabe et al. [14] investigate the mechanical properties of sandwich structures made from PLA using FDM 3D printing, focusing on rhombus and honeycomb core shapes. The functional properties through shape evaluations and conducted tensile, three-point bending, and compression tests were quantified. Results indicate that rhombus structures outperform honeycomb cores, exhibiting increases in tensile, bending, and compression strengths of 15.3%, 39.8%, and 35.1%, respectively, highlighting their superior mechanical performance. Solaiprakash and et al. [15] focuses on the mechanical characterization of honeycomb sandwich structures fabricated using advanced 3D printing technology with continuous carbon fibers and ONYX-FR matrix materials. Edgewise and flatwise compression tests were performed on various configurations, revealing that a face sheet thickness of 3.2 mm and a core cell size of 12.7 mm provided optimal energy absorption and minimized delamination and debonding failures. The findings suggest that 3D printing is a viable method for creating robust sandwich structures, though further parametric studies are needed for broader structural integrity assessments. Harri and et al. [16] explored sandwich panels featuring a 3D-printed gyroid core and carbon fiber-reinforced polymer (CFRP) skin, inspired by the structure found in butterfly wings. Utilizing a FFF printer, gyroid cores with relative densities of 10%, 15%, and 20% were created using PLA filament. Flexural and compression tests revealed that increased core density enhances flexural characteristics and mechanical properties. Additionally, incorporating polyurethane foam improved deflection and sustained load post-fracture, though the unfilled gyroid cores demonstrated superior strength and energy absorption at equal densities. Morettini et al. [17] conducted a comprehensive assessment of the mechanical and physical properties of PLA structures printed using FFF-3D printing. Aimed at enhancing finite element modeling accuracy for predicting component behavior, the study

reveals an ultimate tensile strength of 57.15 MPa, an elastic modulus of 2606 MPa, and a fatigue limit of 13.5 MPa at cycles for horizontally molded specimens. Yonezawa et al. [18] investigate the degradation of mechanical properties in FFF (i.e., Fused Filament Fabrication) 3D-printed PLA structures. Uniaxial tensile and four-point flexural tests on PLA test pieces printed with varying parameters reveal significant changes in mechanical properties after immersion in saline for 30, 60, or 90 days. The study underscores the influence of fabrication parameters on property evolution and offers insights for designing durable FFF-printed structures. Ernst et al. [19] explore the fabrication of small porous structures using Fused Filament Fabrication with an Ultimaker 3, focusing on polymer compounds like PLA, PLA with carbon nanotubes, and polyvinyl alcohol with titanium dioxide. The study investigates the influence of calibration, layer heights, and particulate additives on the printing behavior and accuracy of single-printed lines. Results indicate that small porous structures of PLA/CNT with a line width of 200 µm can be achieved with a layer height of 100 µm per layer yielding optimal component quality. Mostafa et al. [20] explored the impact of equi-biaxial fabric prestressing on the tensile properties of woven E-glass/polyester composites. Using a specialized prestressing apparatus, the study applied tension ranging from zero to 100 MPa during the curing process of plain-weave fabric composites. Tensile tests across various orientation angles revealed that fabric prestressing significantly improved elastic modulus and critical stress to first fracture by 10–20%. Optimal tensile performance, including modulus and critical stress, was achieved at 50 MPa of prestressing, while maximum tensile-limited toughness occurred at approximately 75 MPa of fabric prestressing. Tang et al. [21] investigate the mechanical properties of 3D printed PLA lattice structures and discuss the impact of process parameters. Results reveal that increasing printing temperature initially enhances tensile strength and elastic modulus, peaking at 230 °C with a maximum strength of 50.16 MPa and modulus of 4340.38 MPa. Conversely, yield strength, plastic platform stress, and densification strain of lattice structures decrease with temperature. Monkova et al. [22] explore the sound reflection properties of 3D-printed open-porous PLA structures, including Cartesian, octagonal, rhomboid, and starlit designs. Findings reveal that sound reflection is influenced by structure type, porosity, and thickness, with starlit structures exhibiting lower reflection due to complex pore shapes. Additionally, thinner, highly porous samples without air gaps demonstrate higher sound reflection, especially at low excitation frequencies. Zhao et al. [23] present a study on residual stress in 3D-printed porous PLA structures, which are crucial in medical applications for their mechanical properties. The research establishes a development model correlating residual stress with the stress concentration coefficient. Results reveal a consistent relationship between pore size and surface residual stress, confirming the accuracy of theoretical modeling. The study provides essential guidance for 3D printing porous structures, addressing quality issues arising from residual stress. Khosravani et al. [24] investigate the failure of 3D-printed PLA components. They simulate environmental conditions and assess the impact of accelerated thermal aging on mechanical behavior. Results reveal the influence of thermal aging on structural integrity, offering insights for future design and computational modeling of 3D-printed polymer parts.

This study presents a novel approach to enhancing the mechanical properties of printed PLA sheets through the incorporation of an aluminum layer as reinforcement. By fabricating three-layer samples composed of two outer PLA layers sandwiching a central aluminum layer, it's an innovative composite structure that distinguishes this work from existing research. The key parameters, including the thickness of the aluminum sheet and the size and number of perforations within it, to assess their impact on the mechanical strength of the multi-layered composites. Comprehensive flexural, compression, and impact tests were performed on the resulting samples, providing valuable insights into the performance improvements achievable through this unique reinforcement strategy.

2 Experimental method

2.1 Sample preparation

Initially, aluminium sheets with thicknesses of 1 and 2 mm were cut into dimensions of 75 × 35 mm to reinforce the multi-layer sheets. Additionally, to improve interface adhesion and facilitate bonding between the layers, perforations were created on AA1050 aluminum alloy sheets with 5- and 7-mm diameters, the number and diameters of holes is chosen based on the length and width of the aluminum sheet. The surface of the aluminium sheet was roughened using sandpaper and metal brushes to enhance the adhesion of the printed layers. Figure 1 illustrates some aluminium sheets, depicting the scratches alongside the perforations created on them.

Given that the final dimensions of the sample are 80 × 40 × 10 mm, two-layer components were designed such that the aluminium sheet is embedded after printing the bottom layer, followed by printing the top layer. All samples were printed

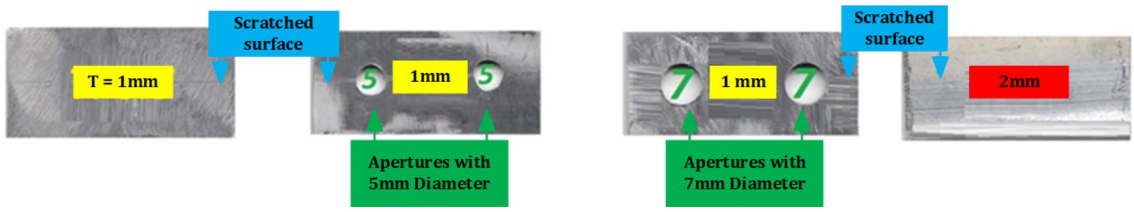

Fig. 1 Images of some prepared aluminum sheets

in two stages, but their print designs and layouts were different. First, the lower layer was printed, and after a brief pause of a few seconds by the printer, the aluminum middle layer was placed within the lower layer, and immediately afterward, printing of the upper layer began to avoid any issues related to adhesion between layers and temperature reduction. The difference in sample production lies in the design of the upper layer, which varies based on the sample and the number and diameter of the holes created in the aluminum sheet. The quality of the final samples is significantly influenced by parameters related to printing PLA filaments. Exceeding the temperature limits can disrupt the part's shape, leading to improper bonding between layers. Finally, the samples were produced at a nozzle temperature of 210 °C and a build plate temperature of 60 °C, with a nozzle diameter of 0.3 mm. To enhance the adhesion between the printed layers and the adjacent paths, smaller nozzle diameters can be used. Although selecting a smaller nozzle diameter increases the print time, a suitable value must be chosen to achieve both maximum quality and minimum print time. In this research, considering the presence of an aluminum layer in the middle of the part, a 0.3mm nozzle was used to improve inter-layer adhesion. Therefore, a nozzle diameter of 0.3 mm was selected for printing the samples [25]. Additionally, alongside the mentioned aspects related to the nozzle, it should be noted that the thickness of the printed layers was set to 0.2 mm, and the number of outer filled layers was 2. The samples were printed with an infill density of 15% and a triangular pattern at a speed of 30 mm/s. Figure 2 depicts the configuration of the final specimen layers and the samples that were produced. Table 1 provides the specifications of all produced samples.

2.2 Mechanical testing

Mechanical tests play a pivotal role in the design and production processes, aiding in the identification of material properties. Common mechanical tests include flexural, compression, and impact tests. The flexural test assesses the sample's flexural

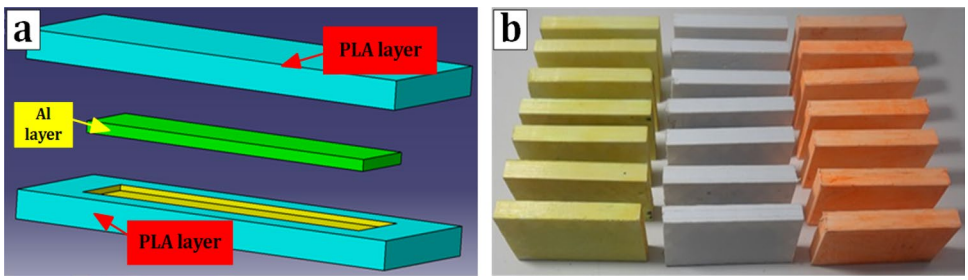

Fig. 2 **a** Multi-layer sheet Sketch, **b** all produced samples

Table 1 Specifications of produced samples

Sample name	Thickness of first PLA layer (mm)	Al middle layer			Thickness of last PLA layer (mm)	Total thickness of final sheet
		Thickness (mm)	Number of perforations	Diameter of perforations (mm)		
S(0,0)	5	–	–	–	5	10
S(1,0)	4.5	1	0	–	4.5	10
S(1,5)	4.5	1	2	5	4.5	10
S(1,7)	4.5	1	2	7	4.5	10
S(2,0)	4	2	0	–	4	10
S(2,5)	4	2	2	5	4	10
S(2,7)	4	2	2	7	4	10

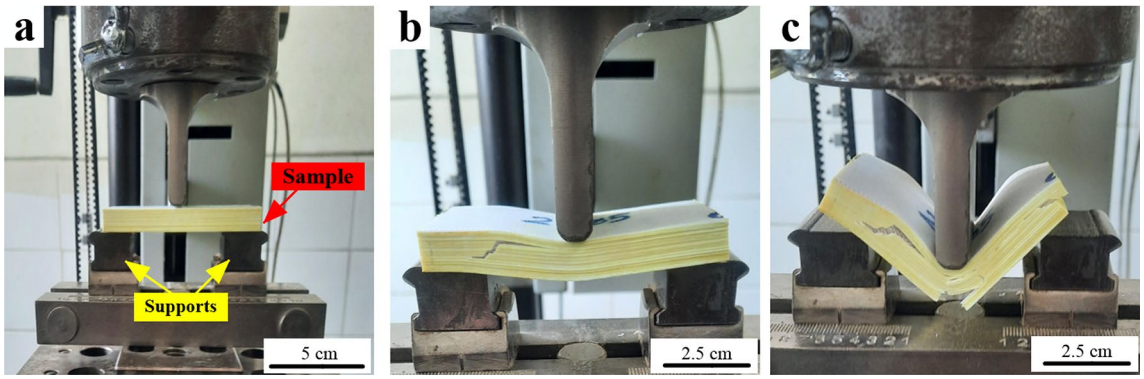

Fig. 3. 3-Point bending test: **a** test configuration, **b** during the test, and **c** fractured sample

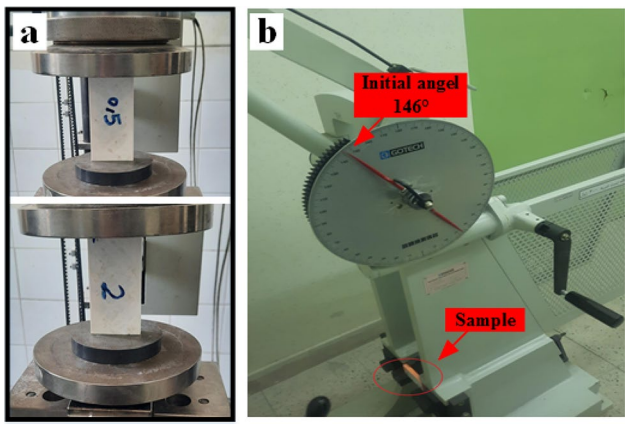

Fig. 4 **a** Compression test, and **b** impact test devices

strength. In this study, the three-point bending test was conducted using a universal machine with a cross-head speed of 5 mm/min, in accordance with the ASTM D790 standard, it should be noted again that the dimensions of the samples differ from the standard, and only the conditions for conducting the test were performed according to the standard. Figure 3 showcases images related to the flexural test. On the other hand, the compression test serves as a criterion to assess the compressive strength of multi-layer samples. The test protocol followed the ASTM D695 standard.

Additionally, to ensure accurate testing and create frictional force, lubrication was intentionally omitted between the surfaces of the sample and the applied force. Finally, the Charpy impact test was conducted on the specimens to determine impact energy and fracture toughness. During this test, the sample is positioned between two supports and a pendulum is inserted into the middle of the sample. The amount of impact energy absorbed by the sample is calculated based on the difference between the primary and secondary angles of the pendulum. The impact test adhered to the ASTM D695 standard, utilizing a pendulum with a mass of 27.24 kg, the height of the drop test of 0.61 m, resulting in an impact speed of approximately 3.5 m/s. The pendulum was released at a primary angle of 146 degrees, and the secondary angle was measured. Subsequently, the impact strength of the sample was calculated using Eq. (1):

$$a_{iu} = E'/b \times h \tag{1}$$

where a_{iu} represents the impact strength of the sample [J/m^2], E' denotes the energy loss [J], and b and h signify the width and thickness [m] of the sample's cross-sectional area, respectively. Images related to the compression and impact tests are depicted in Fig. 4.

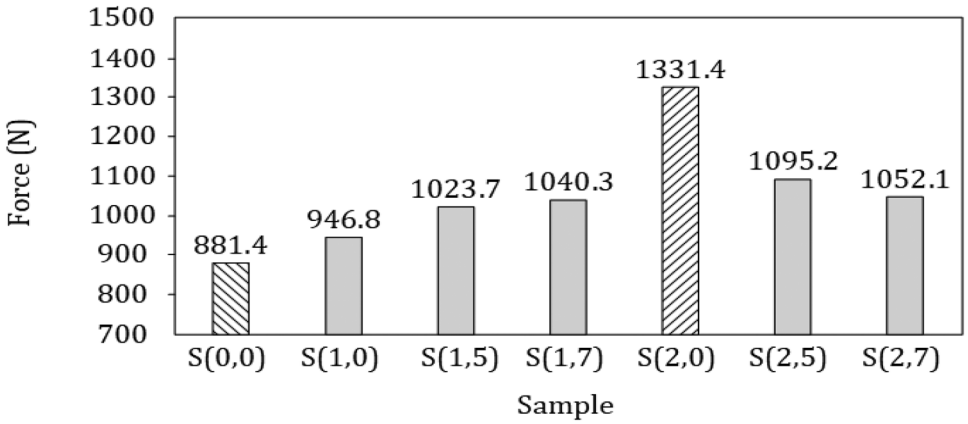

Fig. 5 Flexural test result

3 Results and discussion

3.1 Flexural test

The flexural testing aimed to determine the flexural strength of the multi-layer samples, utilizing a pre-force of 2 N and a cross-head speed of 5 mm/min. The results, depicted in Fig. 5, showcased that the S(2,0) sample demonstrated the highest force at the breakpoint, measuring 1331.4 N, a remarkable 51% higher than the S(0,0) sample. This enhancement is due to the presence of the 2 mm-thick aluminium sheet and the strong adhesion between the layers. Generally, samples reinforced with 2 mm-thick aluminium sheets exhibited the highest force at the breaking point. Moreover, the breaking force decreased as the perforation diameter increased, resulting in decreasing the cross section area of Aluminum sheet.

In contrast, reinforced samples with a 1 mm-thick aluminium layer displayed a different trend. Sample S(1,7) demonstrated a breaking force of 1040.3 N. Enhanced adhesion between the layers, facilitated by larger perforations, improved bonding among the three layers: the upper and lower PLA layers and the aluminium sheet. Consequently, this improvement led to increased force at the breakpoint compared to S(1,5) and S(1,0), with breaking forces of 1023.7 N and 946.8 N, respectively. The force–deflection diagram for the samples under study is illustrated in Fig. 6. The overall trend illustrated in this diagram remains consistent, reaching the maximum force. The fluctuations noted post-peak are linked to both the failure of the PLA layers and the subsequent detachment between the aluminum and PLA layers. Specifically, the initial drop in force correlates with the separation of the aluminum sheet from the printed layers, signifying each force variation as indicative of the separation between successive printed layers. As well, in the sample without aluminium middle layer S(0,0), a sudden decrease occurred as the outermost layer failed under applied loading, with no prior occurrence of layer separation.

The strain of the samples falls within the range of 1% to 4%, with the S(2,0) sample exhibiting the highest strain of 3.8%. Conversely, the S(0,0) sample recorded the lowest strain of 1.4%, indicative of the PLA material's inherent properties and the impact of the added aluminium layers, which contribute to increased flexibility and strength. Images of the fractured

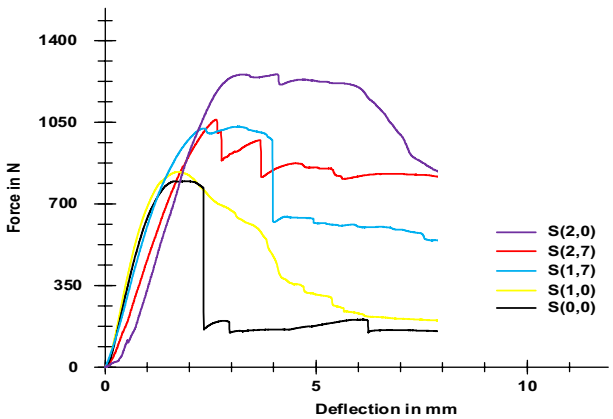

Fig. 6 Force–deflection diagram of multi-layer samples

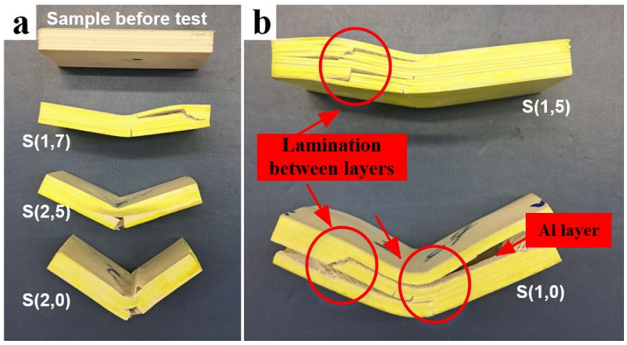

Fig. 7 Fractured cross-section of samples after flexural testing

specimens were captured, as illustrated in Fig. 7, to assess the fracture results. In Fig. 7a, images depict one typical specimen before and three different specimens after the flexural test. For instance, sample S(1,7) exhibited delamination on the compressive side, with visible crack initiation and failure on the tension side. Furthermore, with increasing the flexural strength, no visible delamination occurred, indicating enhanced interlayer bonding; sample failure primarily occurred in the section subjected to the highest tensile force. Also, the fractured surface depict the ductility of the PLA and interlayer cracks were visible on the broken surface, revealing the strong bonding layers [26]. In Fig. 7b, images of specimens with the lowest bending strength are displayed. In sample S(1,5), delamination has occurred both at the top and bottom, specifically at the junction of the Al sheet where the PLA sheets are in contact. This phenomenon was more pronounced in sample S(1,0), where complete separation of the Al sheet resulted from inadequate adhesion between the Al sheet and PLA layers [27]. To further analyze the performance of the S(2,0) sample, which shows the highest flexural strength, images of the fracture of the specimens are provided in Fig. 8. The absence of layer delamination indicates proper adhesion. However, the layers were wrinkled due to the applied force [28]. Additionally, in samples reinforced with 1mm thick aluminum sheets, increasing the hole diameter led to a slight change in the increase of bending strength. However, with thicker aluminum sheets and an increased distance between the top and bottom layers of the print, increasing the hole diameter resulted in a decrease in bending strength. This reduction could be attributed to lower adhesion between the PLA layers due to the increased thickness of the aluminum sheet. Since one of the most important advantages of producing samples using 3D printing is the repeatability of the parts. If production parameters such as filament, fill percentage, temperature, and print speed remain constant, the mechanical properties of the samples will not significantly change [28]. There are some investigations that reported high accuracy and repeatability in parts produced using FFF method in mechanical, chemical properties as well as dimensional error of printed samples with the 3D model. This is indicating a high degree of similarity between the produced parts [29, 30]. In this study, to ensure this, a random repeatability test was conducted on samples S(0,0) and S(2,7), and the maximum difference in bending strength results of the samples was found to be 3%. As a result, further tests were not conducted for other samples.

3.2 Compression test

The compression test was conducted on the multi-layer samples, which were positioned vertically in the machine, with a pre-load of 2 N and a cross-head speed of 5 mm/min. The results are presented in Fig. 9. The maximum force for the S(2,7) sample was determined to be 3672.8 N, representing a 41% increase compared to the S(0,0) sample, which exhibited a force of 2595.2 N. Indeed, the inclusion of an aluminium sheet in the multi-layer sample led to an increase in the maximum compressive force. This increase in force is due to the presence of the aluminium sheet, which enhances the sample's strength against compressive force.

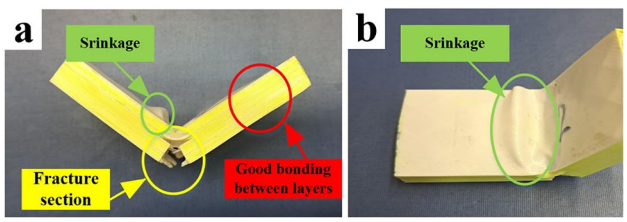

Fig. 8 Fracture of the sample S(2,0): **a** front view, **b** top view

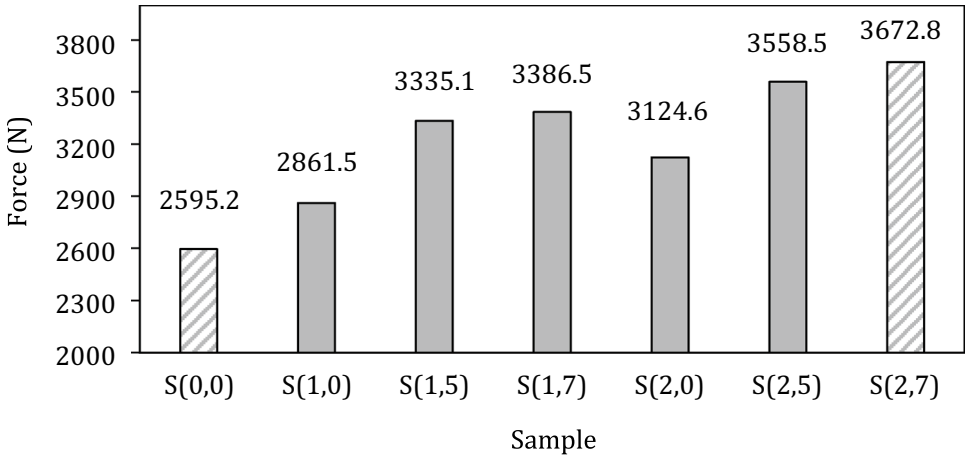

Fig. 9 Compression test result

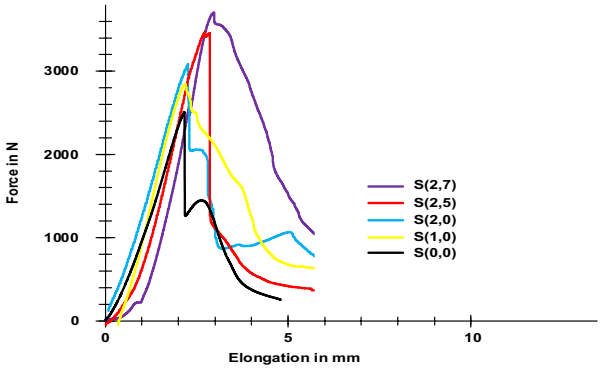

Fig. 10 Force–displacement curve of multi-layer samples

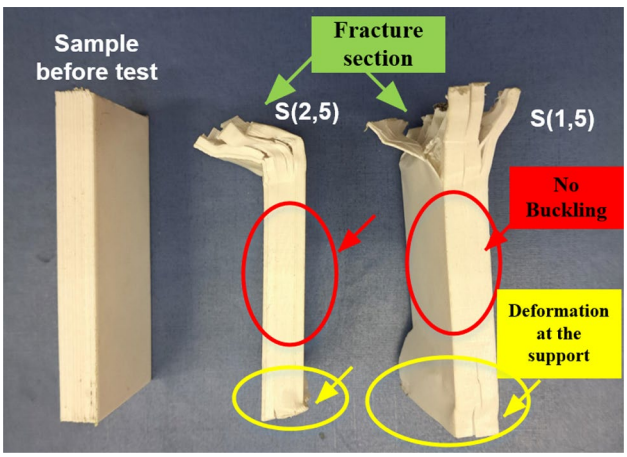

Fig. 11 Fracture surface of produced samples (1,5) and (2,5)

Moreover, the maximum force for samples with solid aluminium sheets was observed to be lower than for samples reinforced with perforated aluminium sheets. Accordingly, the increase in perforation diameter contributed to a higher force. This phenomenon is due to the establishment of bonding between the aluminium layers and the printed PLA layers. Figure 10 illustrates the force–displacement curve of multi-layer samples for the compression test. To evaluate the performance of the produced multi-layer samples under compressive forces, photographs were captured of two samples (1,5) and (2,5), as shown in Fig. 11. The strong connection between the layers prevented any delamination during the test. However, due to the existence of the force reaction, wrinkled deformation occurred at the end of the sample in contact with the support. Nevertheless, failure in the specimens observed at the mid-parts upon compressive force application, resulting in the samples fracture.

Table 2 Impact test results

Sample name	Primary angle	Secondary angle	Energy loss (J)	Impact strength (J/m^2)
S(0,0)	146°	143	0.5	12.5
S(1,0)		127	3.73	93.25
S(1,5)		135	2.0	50
S(1,7)		138	1.41	35.25
S(2,0)		122	4.91	122.75
S(2,5)		125	4.19	104.75
S(2,7)		131	2.84	71

3.3 Impact test

The Charpy impact test was conducted with the primary angle of the pendulum set to 146°. The secondary angle after hitting the sample was measured, and based on these two angles, the energy loss of the pendulum was calculated. The results are summarized in Table 2: The highest impact strength was observed for the S(2,0) sample, reaching 122.75 J/m^2, which represented an increase of 882% compared to the S(0,0) sample. On the other hand, the impact strength of the S(2,5) and S(2,7) samples was determined to be 104.75 J/m^2 and 71 J/m^2, respectively. For the S(2,0) sample, the minimum secondary angle of the pendulum was found to be 122°, with a corresponding energy loss of 4.91 J. In fact, the presence of a 2 mm aluminium sheet without perforations leads to maximized absorbing energy.

In contrast, the secondary angle in the S(0,0) sample reached 143 degrees, only 3° less than the primary pendulum angle. The energy loss of the sample was only 0.5 J, reflecting the low fracture toughness of the pure PLA material. Generally, samples reinforced with a 2 mm aluminium sheet exhibited higher energy absorption than those with a 1 mm sheet. Furthermore, as the diameter of the perforations increased, the impact energy decreased. This phenomenon could be attributed to the increased stress concentration in these samples, resulting from reducing the effective cross-sectional area against the pendulum impact [31].

4 Conclusions

This study aims to investigate how variations in aluminium sheet parameters (such as sheet thickness, number, and perforation diameter) impact the mechanical properties of Fibre Metal Laminate specimens fabricated using 3D printing. PLA sheets were printed on both sides of aluminium sheets, creating a sandwich structure that enhances strength and flexibility. Different thicknesses of aluminium sheets (1 and 2 mm) with perforations of varying diameters (5 and 7 mm) were explored. Subsequently, the samples underwent flexural, compression, and impact tests to evaluate their performance. The findings reveal that:

1. The flexural test results revealed that samples reinforced with 2mm-thick aluminum sheets exhibited significantly higher force at the breaking point than those without aluminium-reinforced sheets.
2. Enhanced adhesion between layers, especially in samples with larger perforations, led to improved bonding and increased force at the breaking point for samples with 1mm-thick aluminium layers during 3-point bending tests.
3. Compression testing showed that the inclusion of aluminium sheets in Multi-layer samples increased the maximum compressive force, with perforated sheets contributing to higher forces due to improved bonding with PLA layers.
4. Charpy impact testing demonstrated that samples reinforced with 2 mm aluminium sheets exhibited higher energy absorption. For instance, the sample featuring a 2 mm aluminium middle layer and a 7 mm perforation displayed an impressive 882% increase in impact strength compared to the sample without aluminium middle layer.
5. The impact energy decreased with increasing perforation diameter, indicating increased stress concentration in samples with larger perforations, affecting their ability to absorb energy efficiently.

Author contributions AS: Idea, Managing and analysis data. AHR and AN: writing and revising. KR and JH: samples' production BD: Doing experimental tests.

Availability of data and materials The raw/processed data required to reproduce these findings cannot be shared at this time as the data also forms part of an ongoing study. These authors are currently working on the effect of other parameters on the material properties.

Declarations

Competing interests The authors declare that they have no competing interests.

References

1. Zal V, Moslemi Naeini H, Konarang M, Roohi AH. An experimental investigation on the laser forming of aluminum/epoxy/glass FMLs. Lasers Manuf Mater Process. 2024;11(2):402–18.
2. Bolat Ç, Ergene B, Ispartalı H. A comparative analysis of the effect of post production treatments and layer thickness on tensile and impact properties of additively manufactured polymers. Int Polym Proc. 2023;38(2):244–56.
3. Yalçın B, Ergene B, Karakılınç U. Modal and stress analysis of cellular structures produced with additive manufacturing by finite element analysis (FEA). Acad Perspect Procedia. 2018;1(1):263–72.
4. Ergene B, Yalçın B. Eriyik yığma modelleme (EYM) ile üretilen çeşitli hücresel yapıların mekanik performanslarının incelenmesi. Gazi Üniversitesi Mühendislik Mimarlık Fakültesi Dergisi. 2023;38(1):201–18.
5. Antony S, Cherouat A, Montay G. Fabrication and characterization of hemp fibre based 3D printed honeycomb sandwich structure by FDM process. Appl Compos Mater. 2020;27(6):935–53.
6. Paul Christopher JE, Sultan MTH, Selvan CP, Irulappasamy S, Mustapha F, Basri AA, Safri SNA. Manufacturing challenges in self-healing technology for polymer composites—a review. J Mater Res Technol. 2020;9(4):7370–9.
7. Liu Z, Lei Q, Xing S. Mechanical characteristics of wood, ceramic, metal and carbon fiber-based PLA composites fabricated by FDM. J Market Res. 2019;8(5):3741–51.
8. Sargini MIM, Masood SH, Palanisamy S, Jayamani E, Kapoor A. Additive manufacturing of an automotive brake pedal by metal fused deposition modelling. Mater Today Proc. 2021;45:4601–5.
9. Li N, Li Y, Liu S. Rapid prototyping of continuous carbon fiber reinforced polylactic acid composites by 3D printing. J Mater Process Technol. 2016;238:218–25.
10. Li Z, Chen X, Jiang B, Fangyun Lu. Local indentation of aluminum foam core sandwich beams at elevated temperatures. Compos Struct. 2016;145:142–8.
11. Xi H, Tang L, Luo S, Liu Y, Jiang Z, Liu Z. A numerical study of temperature effect on the penetration of aluminum foam sandwich panels under impact. Compos B Eng. 2017;130:217–29.
12. Zal V, Sadooghi A, Hashemi SJ, Rahmani K, Roohi AH, Khodayari H, et al. Experimental study of polyester/fiberglass/stainless steel fiber metal laminates mechanical properties. Arab J Sci Eng. 2024;49(8):11167–79.
13. Al Khawaja H, Alabdouli H, Alqaydi H, Mansour A, Ahmed W, Al Jassmi H, editors. Investigating the mechanical properties of 3D printed components. In: 2020 Advances in Science and Engineering Technology International Conferences (ASET); 2020: IEEE.
14. Faidallah RF, Hanon MM, Szakál Z, Oldal I. Study of the mechanical characteristics of sandwich structures FDM 3D-printed. Acta Polytechnica Hungarica. 2023;20(6):7–26.
15. Vellaisamy S, Munusamy R. Experimental study of 3D printed carbon fibre sandwich structures for lightweight applications. Defence Technol. 2024;36:71–7.
16. Junaedi H, AbdEl-baky MA, AwdAllah MM, Sebaey TA. Mechanical characteristics of sandwich structures with 3D-printed bio-inspired gyroid structure core and carbon fiber-reinforced polymer laminate face-sheet. Polymers. 2024;16(12):1698.
17. Morettini G, Palmieri M, Capponi L, Landi L. Comprehensive characterization of mechanical and physical properties of PLA structures printed by FFF-3D-printing process in different directions. Prog Addit Manuf. 2022;7(5):1111–22.
18. Yonezawa A, Yamada A. Deterioration of the mechanical properties of FFF 3d-printed PLA structures. Inventions. 2020;6(1):1.
19. Ernst MF, Maletzko A, Baumann S, Baumann N, Hübner C, Höhne CC. FFF 3D printing of small porous structures from polymer compounds using the ultimaker 3. Macromol Mater Eng. 2022;307(10):2200095.
20. Mostafa NH, Ismarrubie Z, Sapuan S, Sultan M. Effect of equi-biaxially fabric prestressing on the tensile performance of woven E-glass/polyester reinforced composites. J Reinf Plast Compos. 2016;35(14):1093–103.
21. Tang C, Liu J, Yang Y, Liu Y, Jiang S, Hao W. Effect of process parameters on mechanical properties of 3D printed PLA lattice structures. Compos Part C Open Access. 2020;3: 100076.

22. Monkova K, Vasina M, Monka PP, Vanca J, Kozak D. Effect of 3D-printed PLA structure on sound reflection properties. Polymers. 2022;14(3):413.
23. Zhao L, Jiang Z, Zhang C, Jiang Z. Development model and experimental characterization of residual stress of 3D printing PLA parts with porous structure. Appl Phys A. 2021;127:1–10.
24. Khosravani MR, Božić Ž, Zolfagharian A, Reinicke T. Failure analysis of 3D-printed PLA components: impact of manufacturing defects and thermal ageing. Eng Fail Anal. 2022;136: 106214.
25. Solomon IJ, Sevvel P, Gunasekaran JJMTP. A review on the various processing parameters in FDM. Mater Today Proc. 2021;37:509–14.
26. Kumar MS, Farooq MU, Ross NS, Yang C-H, Kavimani V, Adediran AA. Achieving effective interlayer bonding of PLA parts during the material extrusion process with enhanced mechanical properties. Sci Rep. 2023;13(1):6800.
27. Maqsood N, Rimašauskas M. Tensile and flexural response of 3D printed solid and porous CCFRPC structures and fracture interface study using image processing technique. J Mater Res Technol. 2021;14:731–42.
28. Mariam M, Afendi M, Abdul Majid MS, Ridzuan MJM, Azmi AI, Sultan MTH. Influence of hydrothermal ageing on the mechanical properties of an adhesively bonded joint with different adherends. Compos Part B Eng. 2019;165:572–85.
29. Samykano M, Selvamani SK, Kadirgama K, Ngui WK, Kanagaraj G, Sudhakar KJTIJOAMT. Mechanical property of FDM printed ABS: influence of printing parameters. Int J Adv Manuf Technol. 2019;102:2779–96.
30. Singh J, Singh R, Singh H. Repeatability of linear and radial dimension of ABS replicas fabricated by fused deposition modelling and chemical vapor smoothing process: a case study. Measurement. 2016;94:5–11.
31. Azammi AMN, Sapuan SM, Ishak MR, Sultan MTH. Physical and damping properties of kenaf fibre filled natural rubber/thermoplastic polyurethane composites. Defence Technol. 2020;16(1):29–34.